4ICEGE Thessaloniki-GREECE 2007

4th International Conference on
Earthquake Geotechnical Engineering
June 25-28, 2007
Paper No. 1471

EXPERIMENTAL INVESTIGATION OF GROUTED HELICAL PIERS FOR USE IN FOUNDATION REHABILITATION

Yueying BIAN [1], Tara C. HUTCHINSON[2], Dan WILSON[3], Debra LAEFER[4], Scott BRANDENBERG[5]

ABSTRACT

Rehabilitation of building structures is a critical need facing numerous older urban areas. Foundations underlying many of these structures do not have adequate load capacity to support new demands expected after structural rehabilitation or superstructure replacement. Consequently, practical methods for strengthening existing foundations have the potential for significant impact. This is particularly the case for overloaded or weakened foundations susceptible to seismic loads. In engineering practice, both subsurface grouting and helical piers have been widely used to address these issues and provide strengthening of the foundation. If the solid shaft of a typical helical pier is replaced by a hollow shaft, then the helical piers provide the ability to deliver grout. This combined system is now termed a *grouted helical pier system* (GHPS). Although GHPSs have recently seen use in engineering practice, there is limited test data available to understand the mechanisms of load transfer and the potential load enhancement they provide. Small-scale model centrifuge GHPS tests provide an economical approach to simulate the working mechanisms and properties of the GHPS, avoiding costly full-scale prototype testing. In the research presented herein, grouting and pier placement tools were developed and tested on the large geotechnical centrifuge at UC Davis. Experimental methods and procedures are presented and observations regarding the developed grout bulbs under different conditions are described and analyzed. Physical observation of the test specimens indicates that average grout bulbs diameters of 0.6-1.9 times the helix diameter (D_h) are attainable in the 15-g centrifuge environment. For similar grout mixes 20-50% larger grout bulbs can be attained by only adding 0.7 MPa injection pressure. By rotating the pier during grout installation, the generated grout bulbs' average diameter increased approximately 60-100%.

Keywords: Centrifuge testing, foundation rehabilitation, grouting, helical piers

INTRODUCTION

There are many mid-twentieth century constructed structures in the United States, which are reaching their design life. This has taken its toll on the US infrastructure as a whole, as described in reports such as the American Society of Civil Engineers (ASCE) report card (ASCE, 2005), which rated the nation's infrastructure at an overall D (poor) grade and reported 1.6 trillion USD should be spent over the next five years to alleviate potential problems with the nation's infrastructure. The situation is similar in many regions of Europe, where population increases have stimulated building expansions. Due to the historical value of existing structures and potentially economic reasons, aging structures may be rehabilitated, instead of being demolished. However, these structures are often plagued with potential safety problems. For example, due to degraded material engineering properties, poor or inadequate initial design, and unforeseen load conditions, the foundation of these structures may not meet current building codes. In addition, due to the desired new functionality, older structures may

[1]Graduate student researcher (formerly), Department of Civil and Environmental Engineering, University of California, Irvine, USA.
[2]Associate Professor, Department of Structural Engineering, University of California, San Diego, USA. Corresponding author: tara@ucsd.edu, Phone: +1-858-534-7436, Fax: +1-858-822-2260
[3]Research Faculty, Department of Civil & Environmental Engineering, University of California, Davis, USA.
[4]Lecturer, School of Architecture, Landscape & Civil Engineering, University College Dublin, Ireland
[5]Assistant Professor, Department of Civil and Environmental Engineering, University of California, Los Angeles, USA.

undergo structural renovation with additional structural expansion, which often adds considerably more load demand to the original foundation (Hertlein and Walton, 2000). Finally, with the occurrence of natural hazards, such as earthquakes, older foundations or their underlying soil bed may experience a reduction in strength or stiffness capacity, while the superstructure remains in good condition. In these situations, to continue the use of the superstructure, economic and efficient approaches to rehabilitate the existing or damaged foundation and increase their capacity are needed.

Many aged structures are demolished rather than reused, and new structures are constructed at the same location or at a site nearby the demolished structure. In such a situation, the old foundation may be avoided entirely, it may be removed, or it might be re-used. While avoidance might be the simplest and cheapest option, when location is of premium value it may be the least desirable. Removal is often of interest as a simple solution; however, there are trade-offs between the value of the new structure and the complications and cost of removing the original foundation and associated buried utilities, tunnels, etc. In many situations, rehabilitation of the old foundation has proven to be an economical approach. In this context, methods are needed to rehabilitate the foundation to support the new structural loads with minimum deformation.

In this paper, a foundation rehabilitation technique, termed *grouted helical pier system* (GHPS) is investigated. This technique is a combination of subsurface grouting and helical piers, each of which has been widely used individually in engineering practice. However, in this work it is proposed to use them together. The method has been previously explored by Vickars and Clemence (2000) and Manke (2001), and has also been used in practice (e.g. A.B. Chance, 1991). However, there is little test data available to understand the load transfer mechanisms under a variety of parameters (installation technique, grout and soil characteristics, pier characteristics, etc.). Small-scale (model) centrifuge GHPS testing has been proposed to study the mechanisms of load transfer of the GHPS. The primary objectives of the current research are to develop suitable in-flight grout and pier placement tools and techniques, tailored to these proposed tests, and to evaluate the characteristics of the achieved grout bulbs. Parameters of interest in the centrifuge experiments include: (i) grout type, (ii) grout installation pressure, (iii) pier embedment and (iv) pier torquing. It should be emphasized that this particular method, though not the focus of this paper, would be very valuable in the context of seismic remediation of foundations.

EXPERIMENTAL SETUP AND MODEL CONSTRUCTION

The NEES centrifuge at the University of California, Davis, with an effective radius of 8.5 meters, and available container area of 4.0 m^2, was used for these experiments. It is capable of carrying five-ton payloads to an acceleration of 75-g. The testing presented herein was all performed at a centrifugal acceleration of 15 g. The model container had inside dimensions of 1722 mm (length), 686 mm (width), by 700 mm (height), representing a prototype soil area of over 25 m x 10 m. The prototype depth of over 10 m provided enough space for pier embedment, while minimizing the possibility of any boundary effects. All dimensions presented herein are in prototype units unless stated otherwise. Kutter (1992) provides complete description of centrifuge scaling laws.

Schematics of the centrifuge test plan are provided in Figure 1 and a detailed test matrix provided in Table 1. The model included 16 helical piers and two plain piers, with a driving system consisting of gear motors; racks and driving block; grout chambers; mac valves, which control the delivery of grout; and an air pressure supply. The model helical piers each consist of a brass shaft with an O.D. of 106 mm, an I.D. of 96 mm, a helix diameter of 381 mm, and a helix pitch of 77 mm. Parameters varied in the centrifuge test plan include: (i) grout type, (ii) grout installation pressure, (iii) pier embedment and (iv) pier torque (Table 1).

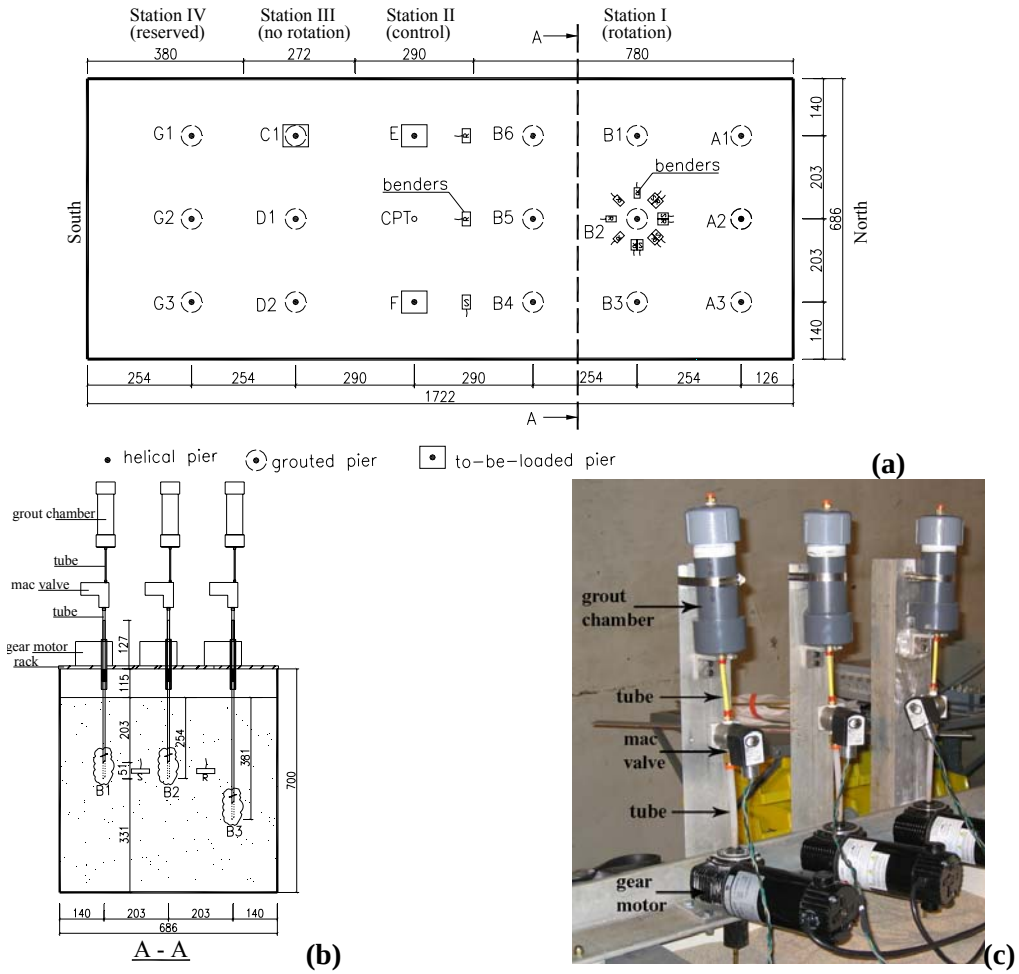

Figure 1. Centrifuge test layout: (a) plan view, (b) section view, and (c) elevation photo of model driving and grouting assembly (units in mm, model scale).

Table 1. Centrifuge Test Matrix.

Table 1. Centrifuge Test Matrix. Pier Location	Helix	Motor rotation @ 5rpm	Embedment depth[1]		Grout Mix				Air Pressure[2] (0.17 MPa)
			3.8m (256mm)	5.7m (381mm)	A	B	C	D	
A1, A2	√	√	√		√				
A3	√	√		√	√				
B1, B2	√	√	√			√			
B3, B4	√	√	√			√			√
B5, B6	√	√		√		√			
C1	√		√		√				
D1	√		√			√			
D2	√		√			√			√
E[3]			√						
F[3]	√		√						
G1	√	√	√				√		
G2	√	√	√				√		√
G3	√	√		√				√	

1. Prototype and model scale embedment depths are both listed, with model scale in parenthesis.
2. Except for marked pier locations, grout is installed under atmospheric pressure.
3. Pier E & F are instrumented with strain gauges for loading test only, no grout installation is performed at these two locations.

The grout mixes used in the centrifuge tests are presented in Table 2. The grout designed for the centrifuge test was based on results from one-g experiments, which demonstrated excellent flowability, relatively long pot life, and high strength (Bian et al., 2006). In addition, grouts are designed with different w/c ratios (0.4-0.6) and additives to improve performance during centrifugal loading. A water reducing agent of between 1-1.5% and between 5-8% silica fume was used to evaluate the potential increase in cohesion of the matrix. For all mixes, Nittetsu Super Fine cement and Mighty-150 water reducer was used.

Table 2. Grout mix summary (percentages by weight of cement).

Grout Mix Type	Water Cement Ratio (w/c)	Silica Fume	Water Reducer
A	0.45	0%	1.5%
B	0.60	0%	1.0%
C	0.40	5%	1.5%
D	0.40	8%	1.5%

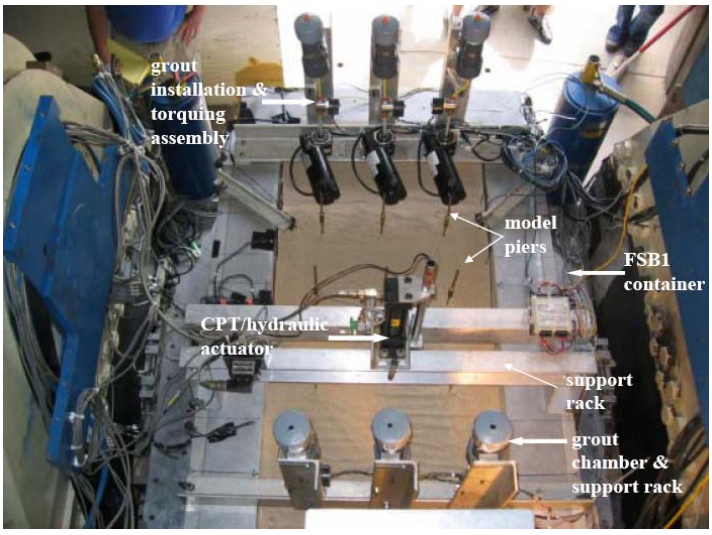

Figure 2. Instrumented model on centrifuge arm.

Model Instrumentation

The centrifuge model was instrumented with strain gauges and bender elements. In addition, an in-flight CPT was performed and a hydraulic actuator equipped with load cell and displacement transducer used during testing. Paired strain gauges were bonded along two pier shafts to measure the friction between the sand and the shaft. Three analog cameras were installed on top of the soil container to capture the images of pier driving, monitor the grout flow in the transparent tubes, and track the pier deformation during the loading tests. The instrumented centrifuge model is depicted in Figure 2.

Two types of benders were embedded in the soil: source benders and receiver benders. The source benders were provided with a voltage excitation from the bender driver and the receiver benders bend and cause a shear wave. The receiver benders then bend by the shear wave and generate a response signal. Thus, shear wave velocity data can be collected along multiple ray paths through the soil, grout and pier as depicted in Figure 3a. In the centrifuge model, one polar array of benders was placed around a pier where a grout bulb was anticipated (pier B2, photograph shown in Figure 3b). The array was placed at a model diameter of 152 mm to assure the benders would not be buried in the grout (the maximum diameter of the grout bulb was estimated to be less than 90 mm). In addition, two rows of free field benders were placed in the soil (at 254 and 381 mm) to evaluate the soil conditions and confirm the hardware functions. The bender system design and validation may be found in Brandenberg et al. (2006).

Soil Profile Characterization

The soil used for the centrifuge model was #30 sand obtained locally from White Cap Construction Supply. The grain size distribution curve indicates the majority of the sand particles are retained on the 50 sieve, with a small percent of fine aggregates present. From the grain size distribution analysis, the Cc and Cu of the sand is determined as 2.32 and 0.79, respectively. According to the Unified Soil Classification System, this type of sand is considered poorly graded. ASTM maximum and minimum density tests (ASTM D 42530-00 and ASTM D 42540-00, respectively), indicate a minimum density of 13.9 kN/m^3 and a maximum density of 16.6 kN/m^3. The sand was placed in the soil container by air pluviation, to obtain a target uniform relative density of 80%. To obtain the target relative density, a steel chamber with known volume and weight was used to calibrate the pluviator. After several trial tests, a relative density of 83.8% was achieved steadily with the soil unit weight of 16.1kN/m^3.

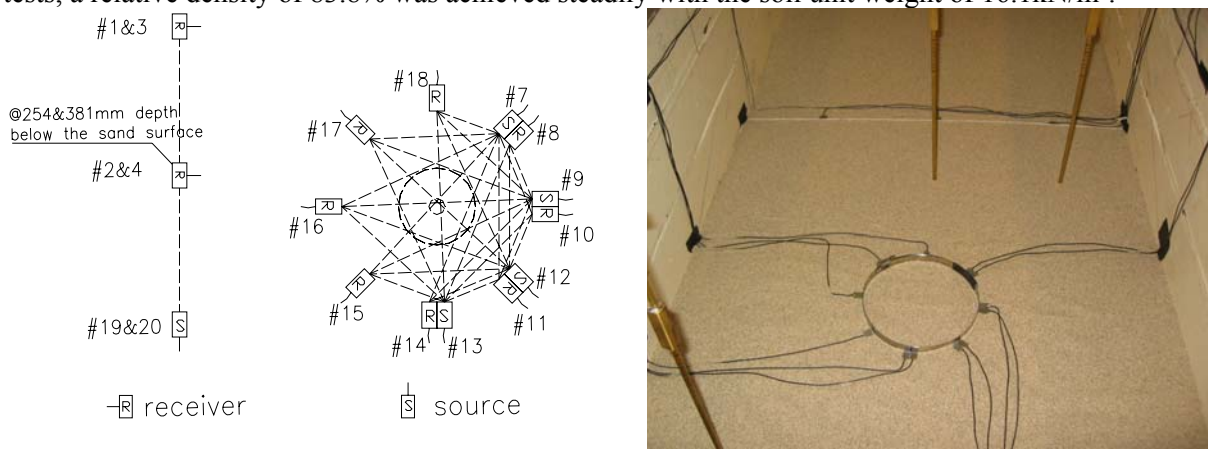

(a) (b)

Figure 3. (a) Bender element ray path traces and (b) photograph of benders in place (Note: the ring is shown for placement of benders only, and was removed prior to testing).

EXPERIMENT EXECUTION, RESULTS AND DISCUSSION

Centrifuge Test Execution

Seven spins were performed in total for this centrifuge test series; complete test series and observations are reported in Bian (2006). Due to the lack of previous work on centrifuge testing of grouted helical piers, the model was carefully monitored during and after each spin and modifications made between spins to improve the grout installation and pier driving. In general, during each spin, three piers were grouted and torqued simultaneously and one pier was grouted without torque.

To minimize the potential for grout hardening prior to completion of the installation, the grout mixing and delivery into the chamber was always the final step before spin up. In the first two spins, grout segregation was observed to be much more severe and faster than that expected. The Nittetsu Super Fine cement grout worked well at one-g without obvious segregation after more than two hours (Bian et al., 2006). It is envisioned that placement of grout at one-g results in sufficient particulate cohesion to inhibit segregation, which appears mainly due to Brownian motion and is slow to develop. However, at 15-g centrifugal acceleration, the cohesion cannot overcomes the centrifugal force, therefore, segregation occurs rapidly and the heavier cement particles are forced out of suspension. To minimize segregation, prior to the third spin, several approaches were attempted. As a first attempt, a funnel was attached to the bottom of each chamber and a larger diameter tube was used to mechanically shorten the grout flow time, while helping guide the grout downward towards the pier and hopefully reducing the grout segregation. Unfortunately, no obvious improvement was observed compared with the former spin results. During the sixth spin, Silica fume was added to the grout mix. The very fine Silica fume particles (medium particle size: 0.5μm) would fill in the spaces between cement grains (median particle size: 3μm), hence reducing the water content and increasing the cohesion between particles. Unfortunately, no substantial improvement due to the addition of Silica fume was observed, due to leakage of the connections at these pier locations. Subsequent testing would further quantify the potential for this improvement.

In-Place Soil Characterization

CPT profiling was conducted in the middle of the container. The CPT probe is capable of penetrating into the sand to a prototype depth of 1.6 m. It should be noted that this is much shallower than the model pier embedment. The CPT extended less than half of the depth of the short pier and one third of the depth of the long pier. However, to characterize the in-place mechanical properties of the sand in the model, published empirical correlations with the CPT data at the deepest measurement point are used. Cone tip resistance may be correlated with relative density as (Kulhawy and Mayne, 1991):

$$D_r^2 = \left(\frac{1}{Q_F}\right)\left[\frac{(q_c / p_a)}{(\sigma_o' / p_a)^{0.5}}\right] \quad (1)$$

where, p_a = atmospheric pressure, σ'_o = vertical effective stress, q_c = cone tip resistance, Q_F = an empirical constant. As suggested in Kulhawy and Mayne (1991), Q_F is selected as 305 for sands with medium compressibility. To use Equation 1, and in light of the shallow penetration of the CPT, the deepest region of measured cone resistance is considered, resulting in a the relative density (Dr) at 1.6 m estimated as 80%, which is consistent with the expected D_r of 84%.

Similarly, an estimate of the in-place strength of the sand may be determined using the relation by Robertson and Campanella (1983):

$$\phi' = \tan^{-1}[0.1 + 0.38 * \log(q_c / \sigma'_0)] \quad (2)$$

Based on Equation 2, the calculated friction angle ranged from 42˚ to 46˚ between the depths of 1.4 m and 1.6 m. For an estimated relative density of 80%, and a friction angle range of between 42˚ and 46˚, the in-place sand for the model may be characterized as dense sand (Meyerhof, 1956).

In-Place Grout Characterization

After placing the premixed grout into each chamber before spinning, the remaining grout was cast into 50 mm diameter cylinders. Compressive strength tests were performed on the same day of the spin, and 18-24 days post-placement. The range of compressive strengths was 23.7-40.7 MPa, with a mean of 30 MPa, and standard deviation of 7.4 MPa. It is noted that these strengths are slightly high for typical grout, yet more comparable to conventional concrete mixes. This high strength may be attributed to the ultra-fine cement and low w/c ratio, which is slightly lower than most field placed grout. However, as noted previously, these mixes performed well at one-g using the pier-sand combinations planned for the centrifuge tests.

Experimental Results

Tomographic Imaging

Tomographic images were constructed before and after grouting while the centrifuge spun at 15-g using a polar array of bender elements placed around pier B2, as shown in Figure 3b. Travel times were picked from the recorded signals, the region between the bender elements was discretized into pixels, and the unknown values of shear wave velocity of the pixels was obtained by tomographic inversion. The resulting tomograms are presented in Figure 4a. The tomograms showed that the shear wave velocity of the soil was uniformly about 210 m/s before grouting, which is fairly reasonable for dense sand. Furthermore, the 38-mm diameter grout bulb (Figure 4b) near the center of the array after grouting was clearly identifiable. The predicted shear wave velocity of the grout (600 m/s) is lower than the expected values (approximately 1570-1800 m/s), and additional studies are needed to identify the cause of this error. Note also that the pixel sizes are large compared with the size of the grout bulb, hence the shape and position of the bulb could not be accurately resolved. A parametric-based approach is being studied to improve these analyses.

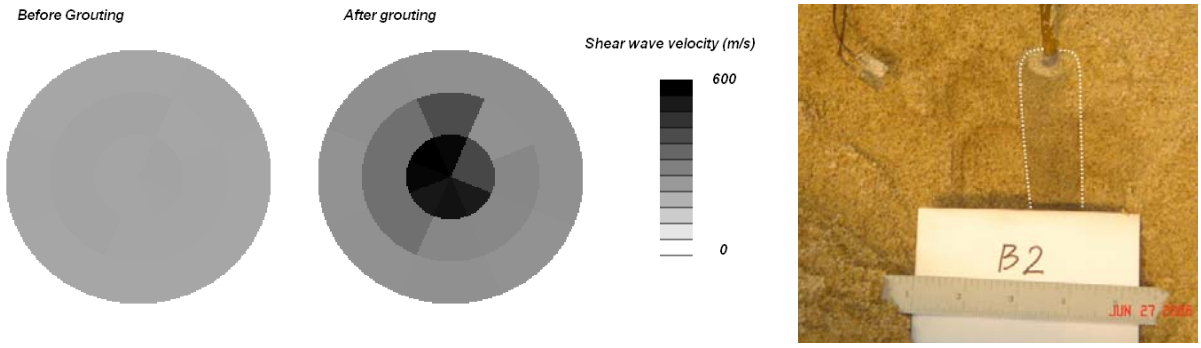

(a) (b)

Figure 4. (a) Tomography depicting shear wave velocity profiles before and after grouting (b) photograph of observed grout bulb at location B2.

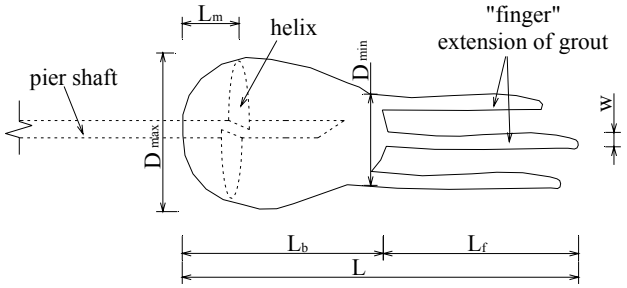

Figure 5. Dimensional analysis of grout bulbs.

Post-Experiment Physical Inspection

Ten days following the final spin, after the grout was thoroughly hardened, the model container was physically excavated and each grouted helical pier carefully removed from the container. Results of the 15 excavated grout installed piers are summarized in Table 3, where the geometric notations used are depicted in Figure 5. Note that dimensions listed in Table 3 are prototype dimensions. It is noted that of the 15 piers grouted, 40% (six) suffered from poor performance of the installation procedure. For example, four helix-pier connections failed during torquing, while two piers suffered from grout leakage during installation, due to a poor seal at the funnel-chamber connection. Despite these failures, much information can be obtained from the successfully grouted piers, as well as those that were unsuccessful, for future testing. Select photographs of the excavated piers and grout bulbs are shown in Figure 6.

In general, the soil-grout bulbs can be characterized by a larger, spherical region surrounding the helix, at the point of grout export, and a region of thinner, 'finger-like' extensions, well below the bottom of the pier. These 'finger-like' extensions tended to extend 2-4 times longer than length of the spherical main body surrounding the helix. The physical size of the 'finger-like' extensions was measured and recorded (L_f) as noted in Table 3. The range of L_f (prototype) was between 38 and 133 cm, generally between one-third and one-half of the total grout bulb length. The total additional weight of grout bulb placed at each pier is also estimated, including the finger extensions, to be between 341 - 721 kg in prototype, excluding those below 100 kg, where physical problems with installation were noted. The maximum grout bulb diameter D_{max} is also recorded and ranged between 14 and 81 cm. The low values (D_{max} = 14 and 19 cm) occurred in those cases where physical problems occurred with the installation (the bottom funnel leaked in this case). It is noted that the range of D_{max} is approximately 0.4 – 2.1 times the helix diameter. Excluding the data from spin six (where funnel leakage was observed), the range of D_{max} is 0.9 to 2.1 times the helix diameter, with an average of 1.5 and standard deviation of 0.5. The length of the major grout bulb (less the finger extensions, noted as L_b) ranged from 67-191 cm (excluding those with physical installation problems). This range generally matched or exceeded the length region over which the target simultaneous grouting and torquing of the piers was conducted (76 cm target draw down depth).

Figure 6. Photographs of excavated grouted piers.

Parametric Study and Discussion

Considering the variables used in the test matrix, embedment depth (L_e), injection pressure (P_i), grout type and the use of rotation, one may perform a parametric study to see how these parameters affected the resulting grout bulbs. In this analysis, the average diameter (D_{ave}) is used to represent the size of the grout bulb, where D_{ave} is taken as $(D_{max}+D_{min})/L_b$ and the weight (W_{GB}) to provide an indication of the overall in-place size. In Figures 7 and 8, the normalized diameter, D_{ave}/D_h, where D_h is the helix diameter; and the normalized weight, W_p/W_{min}, where W_{min} is the minimum grout bulb weight obtained, are used.

In Figure 7a, four scatter plots of L_e versus D_{ave}/D_h are presented, which correspond to four combinations: use of (i) Grout A with rotation, (ii) Grout B with rotation, (iii) Grout A without rotation, and (iv) Grout B without rotation. Figure 7b presents similar data as scatter plots of L_e versus W_p/W_{min}. Results in Figure 7 indicate that under the same soil and grout conditions, the grout bulb diameter D_{ave} ranged between 0.6-1.9 that of the helix diameter, with an average of 1.3 and standard deviation of 0.4. Despite the slight differences in installation, this is fairly consistent with observations by Manke (2001), who noted grout bulbs approximately 0.9-1.2 times the helix diameter. In all embedment cases, Grout A bulbs yielded a larger D_{ave}/D_h value than Grout B bulbs, under both rotation and no-rotation conditions. This may be attributed to the lower w/c ratio of grout mix A (0.45), which also had a consistently higher compressive strength (30-40% greater than grout B). This diameter increase for Grout B, when the piers are rotated (50% increase at 3.8 m depth), is more obvious than that of the non-rotation situation (32% increase at 3.8 m depth). Nonetheless, in all cases, the use of simultaneous rotation and grouting increased the average grout bulb diameter. Furthermore, for greater embedment depths, the grout permeated to a larger diameter. Grout B bulb at 5.7m (L_e = 5.7m) resulted in about a 42% larger diameter than the Grout B bulbs at 3.8 m (L_e = 3.8m). This may be attributed to the larger pressure head applied to the grout.

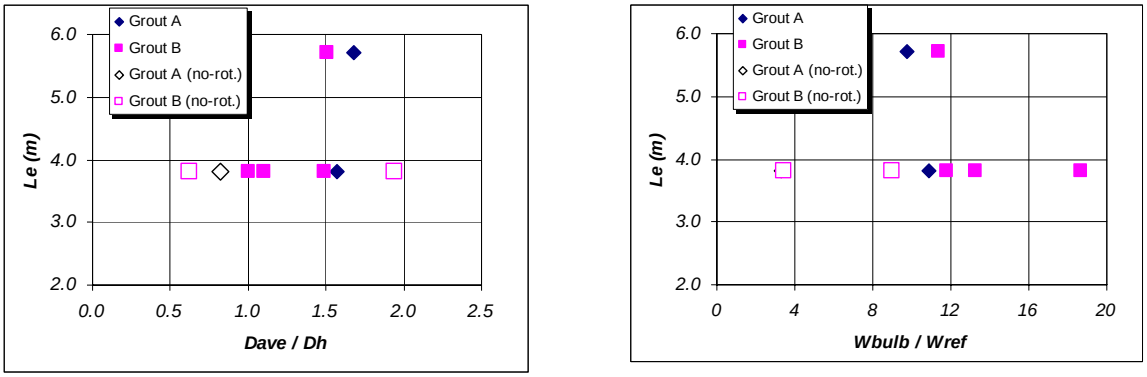

(a) (b)

Figure 7. (a) Normalized grout bulb diameter and (b) normalized grout bulb weight versus embedment depth.

Similar trends may be observed when considering the effects on the final grout bulb weight, as normalized by the minimum grout bulb size, W_p/W_{min}. As observed in Figure 7b, the increase in in-situ bulb weight is sensitive to the depth of embedment, L_e, and is larger for deeper piers. The effect of rotation is also more pronounced, when rotation is included, the final grout bulb weight, shows a 10-12 time increase in W_p/W_{min}. From Figures 7a and b, it is also observed that the same initial volume of grout underwent greater permeation at a deeper pier embedment depth. This results from the injection pressure of the grout at the grout exit hole. The grout injection pressure at the grout exit hole (P_x) is the

sum of the overburden pressure at the exit hole and the injection pressure, $\gamma L_e + P_i$, where γ is the soil dry unit weight, L_e is the embedment depth, and P_i is the added air pressure.

Figures 8a and b are used to study the grout installation performance as a function of the grout injection pressure at the grout exit hole. In Figures 8a and b, the three values of P_x, were the result of: 1) 3.8m embedment depth = 0.16MPa, 2) 3.8m embedment depth plus 0.171 MPa air pressure = 0.19MPA and 3) 5.7m embedment depth = 0.23 MPa. Generally, it is observed from these two figures that for the same type of grout, the grout bulbs under higher injection pressure are larger. Also of note is that although in general, the pier rotation greatly increased the grout permeation, one exception was observed. This case is the outlier at $D_{ave}/D_h = 2.0$ and $W_p/W_{min} = 25.4$, which correspond to the case of Grout B installed without rotation and an injection pressure of 0.23MPa. This case can be attributed to the excessively high injection pressure, which overcame the overburden pressure. Therefore, the grout actually intruded (fractured) the sand mass instead of permeating into the sand voids. In this case, the generated grout bulb was abnormally large.

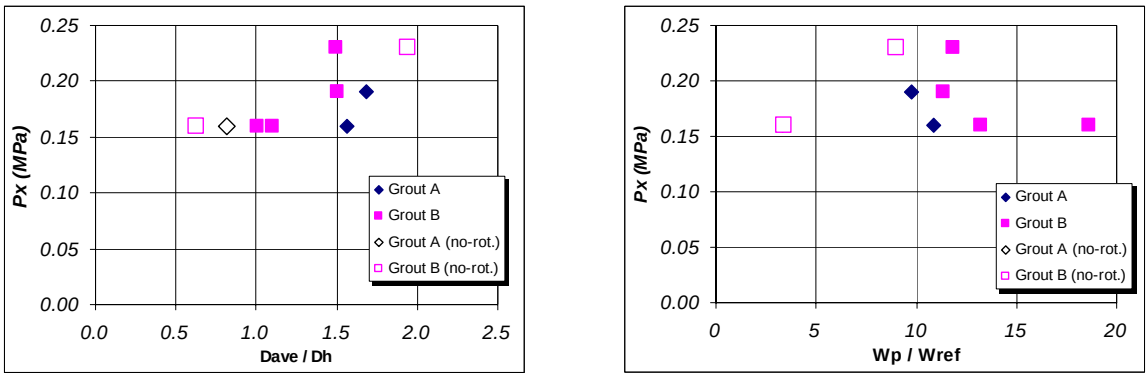

(a) (b)

Figure 8. (a) Normalized grout bulb diameter and (b) normalized grout bulb weight versus injection pressure.

From the parametric study, it is concluded that, first Grout A with a lower w/c ratio generated larger grout bulbs than Grout B, when placed under the same installation conditions, i.e. the embedment depth and the use of rotation; secondly, pier rotation, deeper embedment depth and higher injection pressure all positively improve the grout permeation performance resulting in larger grout bulbs.

Grout Fingering

Grout fingering was observed in the final generated grout bulbs as shown in Figure 6. This phenomenon was not observed in the previous 1-g tests and may be attributed to the increase centrifugal field applied to the model. Here, "fingering" refers to the infiltration of grout mix through the sand in columns of flow. This type of fingering is caused by unstable flow during infiltration into unsaturated homogeneous porous media (Selker et al., 1992; Wang, et al., 2004). A number of theoretical and experimental studies have been conducted to explain the occurrence of fluid instability under different conditions. In the community of hydraulics, one reasonable explanation was proposed by Geiger and Durnford (2000). In their work, an experimental study on the infiltration in homogeneous sands was conducted, and they concluded that a critical flux value exists for fine sands. The authors noted that below this flux value, stable flow occurred, and above this flux, flow was unstable, which resulted in a fingering phenomenon. In the study presented herein, although the pore geometry and permeability remain the same at higher g-levels as that at the 1-g level (Culligan et al., 1997), the grout fluid velocity and the seepage flux are increased by 15 times at 15-g. When the flux value of the grout fluid is larger than the critical flux value of the sand, the grout flow may become unstable. Other explanations have also been proposed for the occurrence of fluid instability, such as the heterogeneity or soil water repellence. To obtain a more quantitative explanation, more theoretical and experimental studies are needed.

One may also estimate the finger's width theoretically, using the approximation for finger extension width (w) proposed by Parlange and Hill (1976):

$$w = \frac{\pi * S_F^{\,2}}{\Delta\theta(K_F - u\Delta\theta)} \tag{3}$$

where, q_s = the flux through the system, q_F = the average finger flux, u = the velocity of the unperturbed flat front, S_F = sorptivity, $\Delta\theta = \theta_F - \theta_0$, θ_F is assumed to be equal to the effective saturated moisture content of the soil. The water content change, $\Delta\theta$, does not vary between model and prototype; therefore, neither will the sorptivity (Culligan et al., 1997). For the dense #30 sand soil, the sorptivity is estimated as 0.72 mm/s^{-2}, therefore, $S_F^2 = 5.2\text{x}10^{-3}$ cm^2/s. Usually, infiltration experiments are carried out to determine the S_F, K_F and $\Delta\theta$. From the literature estimates for K_F = 0.2 cm/s, $\Delta\theta$ = 1, and u = 0.197 cm/s result in w ≈ 5.5 cm (prototype) from Equation 3. After excavation, grout bulbs were observed to have finger extension widths approximately 0.4 cm, which, if multiplied by N=15 (g), results in 6 cm in prototype. This observation is in agreement with the theoretical estimates.

CONCLUSIONS

One promising technique for rehabilitating foundations, which has seen little attention, is the use of the *grouted helical pier system* (GHPS). This paper focuses on developing centrifuge testing tools for the study of the GHPS (or similar systems) in subsequent foundation (seismic or other) rehabilitation studies. In-flight grouting and pier driving were successfully performed simultaneously in the centrifuge testing. In the analysis of centrifuge test results, a parametric study and discussion on the observations regarding the developed grout bulbs under different conditions were studied in detail. Experimental advancements are summarized as follows:

- To address the small scale model requirements on the centrifuge, grout mixes were designed with microfine cement. These mixes provided a sufficiently long pot life and adequate fluidity and strength to permit proper placement through the model pier and permeation through the soil. However, grout segregation was also observed at 15-g due to the inevitable 15-g inertia force. One additive, Silica fume, was suggested to alleviate the segregation.
- A grouted pier in the centrifuge model was instrumented with an array of Bender elements. From the collected results, the relative comparison between the before and after tomographs indicates the presence of a high velocity inclusion, at the grout bulb location. This lends confidence to the use of shear wave tomography in studying, for example, the aerial extent of grouting in-situ during future tests.
- *Parametric analysis* of the grout permeation performance as observed through physical post-experiment excavation reveals that (i) grout bulb diameters ranged between 0.6 and 1.9 times that of the helix diameter (D_h), averaging 1.3 times D_h, (ii) grout with a lower w/c ratio generated larger grout bulbs under comparable installation conditions, (iii) the increase in in-situ bulb size is sensitive to the depth of embedment, and is larger for the deeper piers, (iv) by rotating the pier while grouting, the generated grout bulbs' average diameter increased approximately 60-100%, and (v) for the same type of grout, observed grout bulbs under higher injection pressures are larger, for example, the addition of 0.7 MPa (10psi) air pressure can provide a 20-50% increase in grout bulb diameter and 10 – 45% increase in grout bulb weight.
- A simple study of the *fingering phenomena* observed due to the increased g-field applied to the model indicates that grout with a lower w/c ratio generated longer fingering extensions. While this might be counterintuitive; as one might expect that a more fluid mix would have a greater tendency to be pushed through the soil and flow with the inertial load, in contrast, the lower w/c ratio likely had a greater amount of heavier cement particles in suspension, and this would increase the likelihood for fingering. Furthermore, pier rotation, deeper embedment depth and higher injection pressure all increased the lengths of the observed fingering extensions. Finger extension widths could be reasonably estimated using theoretical methods.

AKNOWLEDGEMENTS

This work was supported by the Civil and Mechanical Systems Division of the U.S. National Science Foundation (NSF) [CMS-0513972], where Dr. Richard Fragaszy is the program director. NEES Operations and Maintenance funding provided assistance with testing costs. Grouted materials were donated by Surecrete, Inc. and DeNeef Construction Chemicals. UC Davis centrifuge staff, in particular Chad Justice and Lars Pederson and input by Dean White of Concrete Technologies and Russell Lindsey of Precision Pier USA, Inc, are appreciated. Opinions, findings, and conclusions in this paper are those of the authors, and do not necessarily reflect those of the sponsoring organization.

REFERENCES

AB Chance Co. "Foundation and underpinning system." BuyLine 1386, A.B. Chance Co., Centralia, MO. (http://www.abchance.com/), 1991.

ASCE, American Society of Civil Engineers, *ASCE report card for America's Infrastructure*. from: http://www.asce.org/reportcard/2005/, 2005.

Bian, Y. *Development and Testing of Centrifuge Tools for Use in Grouted Helical Pier based Foundation Rehabilitation Studies*, MS Thesis, University of California, Irvine. 2006.

Bian, Y, Hutchinson, TC, Wilson, D, and Laefer, D. Grouted Helical Piers for Use in Foundation Rehabilitation: Considerations for Small-Scale Centrifuge Testing. *Proceedings of the International Conference on Re-use of Foundations for Urban Sites* (RuFUS), Garston, UK, 2006.

Brandenberg, SJ, Choi, S, Kutter, BL, Wilson, DW, and Santamarina, JC. "A bender element system for measuring shear wave velocities in centrifuge models", *6th International Conference on Physical Modeling in Geotechnics*, Hong Kong, 1:165 – 170, 2006.

Culligan, PJ, Barry, DA, and Parlange, JY. "Scaling unstable infiltration in the vadose zone." *Canadian Geotechnical Journal*, 34: 466-470, 1997.

Geiger, SL, and Durnford, DS. "Infiltration in homogeneous sands and a mechanistic model of unstable flow." *Soil Science Society of America Journal*, 64: 460–469, 2000.

Hertlein, BH and Walton, WH. "Assessment and reuse of old foundations." *Transport Research Record*, No. 1736: 49-54, 2000.

Kulhawy, FH and Mayne, PW. *Manual on estimating soil properties for foundation design*. Report EL-6800, Electric Power Research Inst., Palo Alto, 306 p., 1990.

Kutter, BL, Dynamic centrifuge modeling of geotechnical structures. *Transportation Research Record*, No. 1336, pp. 24-30, 1992.

Manke, JP. "*Assessment of superposition as a design framework for the combined effects of soil improvement and foundation remediation*." MS Thesis, North Carolina State University, 2001.

Meyerhof, GG. "Penetration tests and bearing capacity of cohesionless soils." *Journal of the Soil Mechanics and Foundation Division, ASCE*, 82(SM1): 1-19, 1956.

Parlange JY and Hill DE. "Theoretical analysis of wetting front instability in soils." *Soil Science*, 122(4):236-239, 1976.

Robertson, PK and Campanella, RG. "Interpretation of cone penetration tests. Part I: Sand." *Canadian Geotechnical Journal*, 20: 718-733: 1983.

Selker, J, Leclerq, P, Parlange, JY, and Steenhuis, T.S. "Fingering flow into two dimensions, 1. Measurement of metric potential." *Water Resources Research*, 28(9): 2513-2512, 1992.

Vickars, RA and Clemence, SP. "Performance of helical piles with grouted shafts." *New Technological and Design Development in Deep Foundations*, N.D. Dennis Jr., R. Castelli and M.W. O'Neill, editors, Geotechnical Special Publication No. 100, ASCE, 327-341, 2000.

Wang, Z, Jury, WA, Tuli, A and Kim, DJ. "Unstable flow during redistribution: controlling factors and practical implications." *Soil Science Society of America Journal*, 3: 549–559, 2004.

Table 3. Centrifuge test results for grout installation (prototype units).[1]

	Pier No.[2]	L_e (m)	P_i [2] (MPa)	P_x (MPa)	Grout Type [3]	Helix Observation	W_g (kg)	Observation after Excavation [4] (cm)						Possible Explanation
								D_{max}	D_{min}	L_m	L_b	L_f	L	
1st Spin	A1	3.8	0.101	0.16	A	helix failed	0	0	0	0	0	0	0	Helix failed & tube leaked.
	A2	3.8	0.101	0.16	A	embedded in grout	570.7	71	48	24	76	130	206	
	A3	5.7	0.101	0.19	A	embedded in grout	587.9	76	52	10	76	133	210	
2nd Spin	B1	3.8	0.101	0.16	B	embedded in grout	341.2	46	38	38	126	122	248	
	B2	3.8	0.101	0.16	B	embedded in grout	402.3	48	29	10	191	84	274	
	B3	3.8	0.171	0.23	B	helix failed	0	0	0	0	0	0	0	Helix failed.
3rd Spin	B4	3.8	0.171	0.23	B	embedded in grout	559.2	69	45	14	110	69	179	
	B5	5.7	0.101	0.19	B	outside the bulb	548.8	67	48	0	69	122	191	
	B6	5.7	0.101	0.19	B	helix failed	0	0	0	0	0	0	0	Helix failed.
1st Spin	C1(*)	3.8	0.101	0.16	A	outside the bulb	47.3	33	29	0	19	38	57	
2nd Spin	D1(*)	3.8	0.171	0.23	B	embedded in grout	721.6	81	67	10	76	122	198	
3rd Spin	D2(*)	3.8	0.101	0.16	B	outside the bulb	28.4	29	19	0	19	38	57	
6th Spin	G1	3.8	0.101	0.16	C	outside the bulb	58.1	14	10	0	30	0	30	Bottom funnel leaked.
	G2	3.8	0.171	0.30	C	helix failed	0.0	0	0	0	0	0	0	Helix failed.
	G3	5.7	0.101	0.19	D	Outside the bulb	81.3	19	11	0	38	0	38	Bottom funnel leaked.

[1] L_e = prototype embedment depth; P_i = grout inject pressure; $P_x = \gamma L_e + P_i$ = total pressure at grout exit hole (γ = soil unit weight: 16.1kN/m^3) W_g = prototype grout bulb weight. All other notations are shown in Figure 5.8.

[2] All piers torqued at target 5 rpm, those noted with (*) were installed grout without rotation